An Analysis-by-Synthesis Approach to Rope Condition Monitoring

Esther-Sabrina Wacker and Joachim Denzler

Chair for Computer Vision, Friedrich Schiller University of Jena
{esther.wacker,joachim.denzler}@uni-jena.de
http://www.inf-cv.uni-jena.de

Abstract. A regular rope quality inspection is compulsory for wire ropes in security-relevant applications. Principal procedures of such quality checks are the visual inspection for surface defect detection, the magnetic inspection for a localization of broken wires and the measurement of the rope diameter. However, until today it is hardly possible for the human inspector to measure other important rope characteristics as the lay length of wires and strands over time. To close this gap, we present a model-based approach for rope parameter estimation. The usage of a theoretically correct and regular 3d rope, embedded in an analysis-by synthesis framework, allows a purely image-based monitoring of important rope parameters. Beyond that, also a quantification of the degree of abnormality becomes possible. Our evaluation on real-world and synthetic reference data demonstrates that the approach allows a measurement of the individual lay lengths of wires and strands up to an accuracy more precise than 1 mm.

1 Introduction

Automatic visual inspection is an arising field of interest. Especially in scenarios, which imply a high risk for the human life or which demand utterly concentration over a long time period, an automatic support is highly appreciated. The inspection of wire ropes used for ropeways, elevators or bridges is one example of such a task. As they are used in security-relevant application areas, a regular quality check is obligatory. Until today, such a quality check is composed of two different parts: the magnetic inspection of wire ropes allows a detection of interrupts or deformations within the wire structure up to a certain extent. However, this method is limited to defects which change the magnetic signal of the wire course. For this reason, the second part is normally a visual inspection of the rope surface by human experts, which is meant to identify all visible anomalies like missing and broken wires or corrosion in the surface structure. Anyhow,

This manuscript is originally published in *Advances in Visual Computing, Lecture Notes in Computer Science, Volume 6454, Springer, 2010, pp 459–468.* The final publication is available at
http://link.springer.com/chapter/10.1007%2F978-3-642-17274-8_45

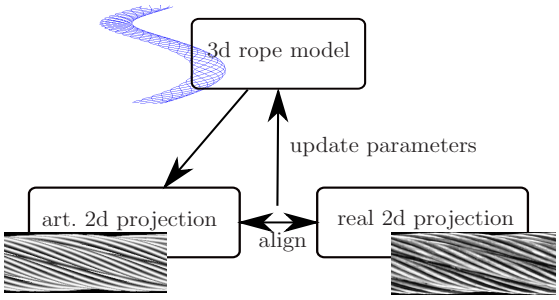

Fig. 1: The general analysis-by-synthesis framework for rope condition monitoring.

none of these inspection methods allows a monitoring of main rope parameters as for example the lay length of strands and wires. And even for a human expert it is an almost impossible challenge to observe creeping changes in the main rope structure, since these variations are not visible to the naked eye. The only way to achieve this would be a manual and repeated measurement which is imprecise and time-consuming. To the best of our knowledge, until today there exists no automatic approach, which provides measurements for the main rope parameters. Nevertheless, a monitoring of these variables could give important and so far unused information about the rope condition.

On this account, we introduce a new, model-based approach for rope condition monitoring embedded in an analysis-by-synthesis framework. The general process chain of our approach is sketched in Fig. 1. Given just the 2d projections of the real-world rope, they are aligned with a perfectly regular and theoretically founded, parametric 3d model. This 3d rope model will be introduced in Sect. 3.1. The 2d/3d alignment is performed by registering an artificially generated 2d projection of the model with the real rope projection. The synthesis procedure for generating artificial 2d projections is introduced in Sec. 3.2. The rope parameters are then updated in an iterative fashion, based on a similarity measure which allows a comparison of the real and synthetic projections.

The periodic rope structure makes great demands on this registration procedure, as it turns the alignment into a complex and highly ambiguous problem. To solve for this problem and to provide an automatic, accurate and combined estimation of individual rope parameters is the main contribution of this work. This optimization strategy is explained in detail in Sect. 3.3. The experiments in Sect. 4 account for the applicability of the presented approach as it provides a very accurate estimation of the actual rope characteristics and enables a surveillance of individual fabrication components. Last but not least, method and payoff are summarized and discussed in Sect. 5.

2 Related Work

Rope Inspection. Most of the work in the field of automatic rope inspection normally makes use of magnetic measurement techniques as described for example in [1] to identify abnormal changes in the specific signal of the wire course. There exists few work coping with automatic approaches for visual rope inspection. As the most important problem in this context is a lack of missing defective examples for supervised learning strategies, Platzer et al. present a one-class classification approach to surface defect detection in wire ropes based on different features [2]. In [3] the same authors make use of Hidden Markov models to solve the problem of defect localization in wire ropes. However, none of these approaches focuses on an automatic estimation of meaningful rope parameters, which would close the gap between all the different inspection techniques.

Analysis-by-Synthesis. Our approach deals with the problem of image-based (2d-based) estimation of time-variant (dynamic) scene parameters. A well-known approach to this problem is analysis-by-synthesis. The parametrized 3d model is adapted to the 2d input image by minimizing the measurable difference between this input image and a synthetically generated projection of the 3d model. The best alignment of model and scene finally results in the parameter estimates.

Typical application examples for analysis-by-synthesis include camera calibration [4] and camera pose estimation [5,6], human motion analysis [7] and (object) tracking applications [8]. A similar concept is used in medical applications such as 2d-3d image registration, where digitally reconstructed radiographs (DRRs) are used to estimate the transformation parameters between 2d images and the corresponding 3d dataset [9].

For rope condition monitoring, analysis-by-synthesis is of particular interest for two reasons: at first, the task of rope condition monitoring can be interpreted as a parameter estimation problem and secondly the alignment with a perfectly regular 3d rope model facilitates the detection and quantification of anomalies with respect to the important rope characteristics.

3 Rope Parameter Estimation

3.1 Parametric 3d Rope Model

The basic prerequisite for the estimation of 3d scene parameters is a parametric 3d rope model. A description of the general rope geometry of wire ropes can be found in many specific literature [10,11]. As for the image-based analysis just the 2d volumetric appearance of the wires is of relevance, a simplified 3d wire centerline model is used for our scope.

In general, a stranded rope consists of wires, which are organized in strands. These strands, in turn, form the entire rope. In the top left of Fig. 2 the fundamental construction of a wire rope is shown: A certain number of strands (big circles) are grouped around the rope core (gray shaded) and each strand consists of an also fixed number of wires (small circles). Both, strands and wires can be

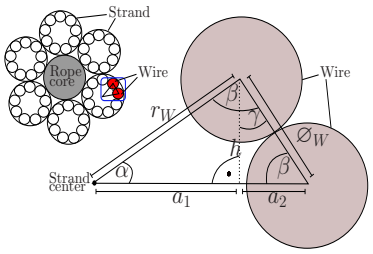

Fig. 2: General rope geometry (top left) and wire geometry (right).

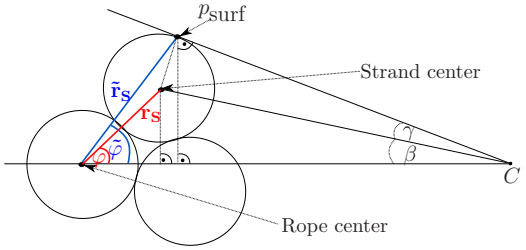

Fig. 3: Geometry for the computation of the model contour of a volumetric rope projection.

described by helix-shaped space curves around the rope or rather strand axis. Taking this into account, we can build a 3d model describing the wire centerlines of the rope. A wire centerline $\boldsymbol{W}_{i,j}$ of wire i in strand j can be described by two intertwined helices, whereas the first helix $\boldsymbol{S}_j$ describes the space curve of strand j and $\boldsymbol{W}_i$ represents the space curve of the wire i. As a line camera is used for the acquisition of the real rope, the rope model is rotated around the y-axis to align the rope axis (time axis) with the x-axis of the camera coordinate system. So, the wire i in strand j can be described as:

$$\boldsymbol{W}_{i,j}(\boldsymbol{p}_S, \boldsymbol{p}_{W_j}, t) = \tag{1}$$
$$\underbrace{\begin{pmatrix} t \\ r_S \sin(t\frac{2\pi}{L_S} + jk_S + o_S) \\ -r_S \cos(t\frac{2\pi}{L_S} + jk_S + o_S) \end{pmatrix}}_{\boldsymbol{S}_j} + \underbrace{\begin{pmatrix} 0 \\ r_W \sin(t\frac{2\pi}{L_{W_j}} + ik_W + o_{W_j}) \\ -r_W \cos(t\frac{2\pi}{L_{W_j}} + ik_W + o_{W_j}) \end{pmatrix}}_{\boldsymbol{W}_i}.$$

Thereby, r_S and r_W are the fix radii of the strand and wire space curves. $jk_S = j\frac{2\pi}{\#S}$ denotes the phase displacement for the j-th strand in the rope and $ik_W = i\frac{2\pi}{\#W}$ is the phase displacement of the i-th wire in each individual strand. $\#S$ is the number of strands in the rope and and $\#W$ the number of wires in a strand respectively. Given these fixed values, the rope can be parametrized by the remaining free and dynamic parameters which are organized in the parameter vectors $\boldsymbol{p}_S = \left(L_S, o_S\right)$ and $\boldsymbol{p}_{W_j} = \left(L_{W_j}, o_{W_j}\right)$. They contain the lay lengths of strands L_S and the lay lengths of wires in the j-th strand L_{W_j} as well as their position o_S and o_{W_j} with respect to the corresponding periods.

The fix radii of the strand and wire space curves r_S, r_W can be computed based on the rope specification. Such a specification normally contains information about the rope and wire diameters $\varnothing_R, \varnothing_W$ as well as the number of strands per rope $\#S$ and wires per strand $\#W$. In Fig. 2 the basic rope geometry is sketched. Applying standard trigonometric operations on this geometry allows the formulation of the radius of the wire space curve as $r_W = \frac{\sin(\beta)\varnothing_W}{\sin(\alpha)}$. The computations for r_S are analog.

3.2 2d Image Synthesis

Given the 3d rope model from Sect. 3.1 an artificial 2d projection can be computed. Since the rope acquisition is done with line cameras [12], also known as pushbroom cameras, the specific projection geometry of this 1d sensor type must be taken into account. The projection matrix for linear pushbroom cameras, which leads to a perspective projection along the sensor array and to an orthographic projection along the time axis, is derived by Gupta and Hartley in [13] under the prerequisite of constant and linear camera motion. In the rope acquisition procedure this is fullfilled, as the camera moves with a constant velocity along the rope axis. According to Gupta and Hartley the pushbroom projection of a 3d rope point $\boldsymbol{W}_{i,j}(\boldsymbol{p}_S, \boldsymbol{p}_{W_j}, t)$ to a 2d point (u, v) can be written as:

$$\begin{pmatrix} u \\ v \end{pmatrix} \leftarrow \begin{pmatrix} u \\ wv \\ w \end{pmatrix} = \underbrace{\begin{pmatrix} 1 & 0 & 0 \\ 0 & f & p_v \\ 0 & 0 & 1 \end{pmatrix}}_{\mathbf{K}} \underbrace{\begin{pmatrix} \frac{1}{V_x} & 0 & 0 \\ \frac{-V_y}{V_x} & 1 & 0 \\ \frac{-V_z}{V_x} & 0 & 1 \end{pmatrix}}_{\mathbf{V}} \left(\boldsymbol{W}_{i,j}(\boldsymbol{p}_S, \boldsymbol{p}_{W_j}, t) + \begin{pmatrix} 0 \\ 0 \\ d \end{pmatrix} \right). \quad (2)$$

Here, d is the unknown but fix camera-to-scene distance. Therefore, the parameter vector $\boldsymbol{p}_S$ is extended by the further free parameter d. We assume that the camera moves one camera line per time step along the rope axis implying $V_x = 1$ and $V_y = V_z = 0$. Also, we have no specific calibration data for the camera, but the 3d rope diameter $\varnothing_R$ as well as the rope diameter in pixels in the real 2d projection $\varnothing_R^{2d}$ are known. Accordingly, a 3d rope point is projected with a focal-length $f = 1$ and a projection center $p_v = 0$. Afterwards, the resulting projection is rescaled to the given 2d rope diameter in pixels. This allows an optimization of the ratio between f and d. The projection of a 3d rope point $\boldsymbol{W}_{i,j}(\boldsymbol{p}_S, \boldsymbol{p}_{W_j}, t)$ in Cartesian coordinates can be given combining (1) and (2):

$$\big(u,\, v\big)^T = \left(t,\, \frac{r_S \sin(t\frac{2\pi}{L_S} + jk_S + o_S) + r_W \sin(t\frac{2\pi}{L_{W_j}} + ik_W + o_{W_j})}{-(r_S \cos(t\frac{2\pi}{L_S} + jk_S + o_S) + r_W \cos(t\frac{2\pi}{L_{W_j}} + ik_W + o_{W_j})) + d} \right)^T. \quad (3)$$

An exemplary 2d wire centerline projection is depicted in the left of Fig. 4. The volumetric wire appearance, which is needed for the alignment process, can be approximated by centering a 1d Gaussian around each projected wire centerline pixel for every time step. The width of the Gaussian mask was based on the projected wire diameter $\varnothing_W^{2d}$ in pixel. A Gaussian seems to be a good choice, as the uncertainty for wire presence slabs with the distance of the pixel to its centerline. The volumetric projection can be seen in the right image of Fig. 4.

3.3 Estimation of Rope Parameters

The parameter optimization is performed in a two-step manner: at first, the strands of the rope model and the real projection are aligned by optimizing the strand parameters included in $\boldsymbol{p}_S$. Afterwards, the wires of each individual strand are aligned, leading to the estimates for the wire parameters $\boldsymbol{p}_{W_j}$ of strand j.

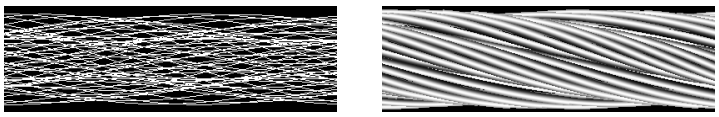

Fig. 4: Synthetic wire centerline projection (left) and volumetric wire projection (right).

A good strategy for a combined alignment of all rope strands is based on the rope contour, as it contains all necessary information. The upper and lower rope contours $c_u^r(t)$ and $c_l^r(t)$ of the real rope are automatically extracted from the real input image. For the upper and lower model contours in the synthetic 2d projection an analytical description can be derived. Figure 3 shows the underlying geometry. The strand center, defined through the angle given by $\varphi_S = t\frac{2\pi}{L_S} + jk_S + o_S$ and the radius of the strand space curve r_S (both marked in red), will lead to a contour point in the 2d *centerline* projection. However, to describe the 3d point p_{surf}, which will lead to a contour point of the *volumetric* 2d rope projection, a new angle $\tilde{\varphi}_S$ and a new distance $\tilde{r}_S$ (marked in blue) can be computed with help of trigonometric operations.

The computation of the 2d projection of a strand centerline $\boldsymbol{S}_j$ (see (1)) with regard to the projection geometry introduced in Sect. 3.2 is straight forward. Hence, we just denote the modified formula using $\tilde{\varphi}_S$, $\tilde{r}_S$ instead of φ_S, r_S:

$$\tilde{\boldsymbol{S}}_j^{2d}(\boldsymbol{p}_S, t) = \begin{pmatrix} t \\ \frac{\tilde{r}_S \sin(\tilde{\varphi}_S)}{-(\tilde{r}_S \cos(\tilde{\varphi}_S))+d} \end{pmatrix} \tag{4}$$

A minimum/maximum operation on the y-coordinates $\tilde{S}y_j^{2d}$ of (4) for all strands in a *time frame* $T = [t_1, t_2]$ leads to the rope contour of the volumetric model:

$$c_u^m(\boldsymbol{p}_S, t) = \min_j \tilde{S}y_j^{2d}(\boldsymbol{p}_S, t), \quad \forall t \in T \tag{5}$$

$$c_l^m(\boldsymbol{p}_S, t) = \max_j \tilde{S}y_j^{2d}(\boldsymbol{p}_S, t), \quad \forall t \in T. \tag{6}$$

The optimization of the parameter vector $\boldsymbol{p}_S$ is performed by evaluating the normalized, 1d cross correlation coefficient $NCC_T^{1d}[\cdot,\cdot]$ of both given contours:

$$\hat{\boldsymbol{p}}_S = \arg\max_{\boldsymbol{p}_S} NCC_T^{1d}\left[c_u^r(t), c_u^m(\boldsymbol{p}_S, t)\right] + NCC_T^{1d}\left[c_l^r(t), c_l^m(\boldsymbol{p}_S, t)\right]. \tag{7}$$

After the determination of the strand parameters, the wire parameters $\boldsymbol{p}_{W_j}$ are estimated in a similar fashion. The optimization procedure is carried out separately for the wires of each individual strand, as their parameters need not necessarily be equal. Instead of the 1d normalized correlation coefficient its 2d counterpart $NCC_T^{2d}[\cdot,\cdot]$ is used to align the image data of real and synthetic rope projections $\mathcal{I}_{real}, \mathcal{I}_{syn}$ for the time frame T:

$$\hat{\boldsymbol{p}}_{W_j} = \arg\max_{\boldsymbol{p}_{W_j}} NCC_T^{2d}\left[\mathcal{I}_{real}, \mathcal{I}_{syn}(\hat{\boldsymbol{p}}_S, \boldsymbol{p}_{W_j}, t)\right]. \tag{8}$$

Both optimization steps make use of the Downhill Simplex optimization scheme [14], whereas a global grid search is put in front of the wire alignment step. This is necessary, as the wire alignment is a highly periodic and therefore ambiguous problem which demands for a good initialization. Although only the strand lay length and the individual wire lay lengths are of interest for the monitoring task, the remaining parameters have to be estimated to achieve a time-variant alignment of strands and wires.

4 Experimental Evaluation

In this section the presented method is validated on real rope data sets. To the best of our knowledge this is the first approach, which allows an automatic estimation of the stated rope parameters. Therefore, we are not able to compare with other approaches. Moreover, a manual measurement of a real rope would be too time-consuming and imprecise, so that it is not possible to compute an estimation error on real-world data. Hence, the quantitative evaluation of the accuracy is assured additionally with help of a simulated ground truth data set. Certainly, this synthetic reference data is computed based on the same ropemodel. Nevertheless, the segmentation and extraction of the rope contour from the reference projection is the critical part of the analysis, which forms the foundation for the parameter estimation. Thus, at first we prove the functional efficiency on real-world data. In the synthetic experiments we then focus on the tracking ability of our approach with respect to creeping parameter variations, as they are a matter of particular interest for (visual) rope inspection.

Real Rope Datasets. The acquired 6×19 seal rope consists of six strands and nine visible, outer wires. It has a length of approximately 3.4 meters, a diameter of 20.46 mm and an expected strand lay length of 137.5 mm. One camera line corresponds to 0.1 mm of rope. Note, that the expected lay length is just an initial guess. It varies around a few millimeters even for intact ropes.

Three different 2d input sequences of the same rope are used. The first one, denoted by **Seq.1**, is the reference sequence. For **Seq.3** the rope was manually untwisted and for **Seq.2** is was re-twisted. This manipulations should primarily result in an altered strand lay length. The parameter tracking results for the strand lay length of these three sequences are displayed in Fig. 5. The manually measured strand reference lay length for some exemplary frames of each sequence is given by the dashed line. This value is 136.6 mm for **Seq.1**, 139.5 mm for **Seq.2** and 133.0 mm. for **Seq.3**. Fig. 5 reveals the following outcomes: at first the approach is capable of clearly identifying the difference in the strand lay length of the three different sequences. Secondly, the variation in the estimation results over time varies around $\pm$ 1 mm which is less then one percent of the measured value. Last but not least, it becomes clear, that the lay length is a time-variant, dynamic parameter for which it is hard to define a reference value by manual measurement. Furthermore, the reader's attention should be drawn to the visible correlation in the lay length course of the three different sequences.

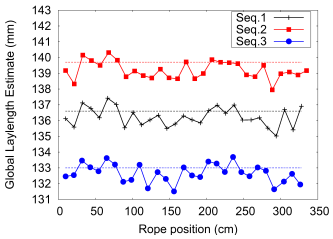

Fig. 5: Strand lay length estimation on the three different real data sequences.

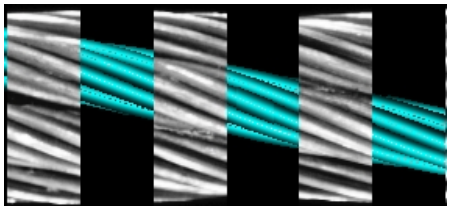

Fig. 6: Registration result: reference (all strands) and model projection are displayed in an alternating fashion.

Fig. 7: Backprojected Strand (white stripes) into the original rope projection.

This is a further indicator for the quality of our estimation results. The variation coefficient (standard deviation/mean) for 10 different estimation runs is 0.0028% for the strand lay length and 3.3% for the wire lay lengths.

Furthermore, the quality of the parameter estimates can be evaluated by backprojecting the model strands and wires to the original 2d projection of the real rope. This allows a visual judgment of the results. Fig. 7 displays the backprojected strand whereas Fig. 6 displays the registration result for the wires of one central strand (blue). In both cases a checkerboard representation, which displays reference image and the backprojected rope model in an alternating fashion (gray and white/colored stripes) is used. As one can see, the strand alignment as well as the wire alignment is very precise. Most of the crossings between real and synthetically generated wires fit almost perfectly together. In the few cases, where the crossings between the wires are not seamless, this can be justified by the fact, that the rope model is a perfectly regular structure whereas this does not hold for the real rope due to manufacturing tolerances.

The computation times achieved on an Intel Core2 (2 MHz) vary around 230 s / m for strand and wire alignment. Note, that currently this is a non-GPU implementation, so that there is a lot of space for performance improvement.

Simulated Ground Truth Data. The simulated rope is composed of six strands and nine wires. For each individual testrun we simulate 30 m rope. The temporal resolution is 0.1 mm per camera line. The ground truth values of all free parameters for every individual testrun are randomly chosen with strand lay lengths from 123 mm to 152 mm and wire lay lengths from 59 mm to 99 mm.

To evaluate the accuracy of the presented approach Gaussian noise with different noiselevels is added to the rope contours and the grayvalues of the

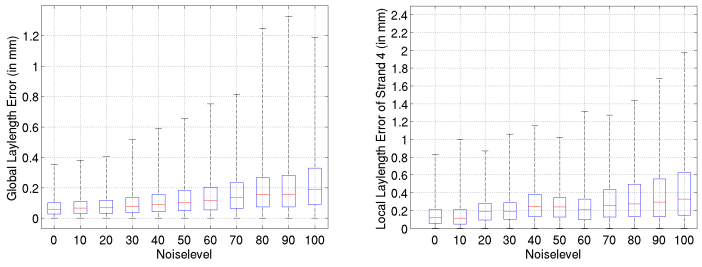

Fig. 8: Boxplots showing the robustness of the lay length estimates of strands (left) and wires (right) to noise.

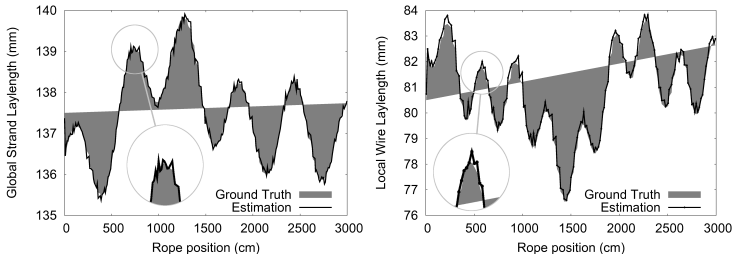

Fig. 9: Parameter tracking of lay lengths for strands (left) and wires (right). The gray curve represents the ground truth parameter progression, the black one the estimates.

ground truth rope projection. The resulting error distributions are visualized by means of boxplots [15]. In Fig. 8 the boxes depict the 0.25 and 0.75 quantiles and the middle bar marks the median error in millimeters obtained for all time steps of 20 randomly initialized test runs per noise level. The left plot shows the results for the strand parameter L_S and the right image illustrates the error distribution for the wire lay length of an exemplary chosen strand. The maximum position errors are around 1.3 mm and the camera-to-scene distance d can be measured with a mean accuracy of ~ 3.7 mm. Although this high accuracy is obtained with respect to a simulated test data set, these results prove the functional capability of our approach.

In order to prove the capability of the approach to track parmeter variations, a randomly generated parameter progression is precomputed for every individual lay length parameter. This progression is marked by the gray curve in the plot of Fig.9. The estimates for every frame resulting from the analysis-by-synthesis loop are represented by the solid, black curve. The high accuracy is also reflected in the low mean errors obtained in 100 randomly initialized test runs. These are 0.06 mm for the strand lay length and 0.23 mm for the wire lay lengths.

5 Conclusions and Outlook

An new approach to image-based rope condition monitoring was presented. With help of an analysis-by-synthesis framework, important rope characteristics as the lay lengths of wires and strands can be measured and a quantification of anomalies becomes possible. Experiments on simulated ground truth data reveal a high accuracy with worst-case estimation errors around 2 mm in the presence of noise. Beyond that, the applicability to real data is attested by the almost perfect alignment of wires of synthetic and real projections. To the best of our knowledge this is the first approach allowing a combined and automatic estimation of strand and wire parameters and thus provides an univocal mapping of a real 2d rope projection and a theoretically perfect 3d rope model.

Besides the parameter monitoring task, an image-based comparison of real and synthetic projections also can be a great benefit with respect to surface defect detection in wire ropes due to the direct comparability of the appearance of each arbitrary wire. This will be the focus of future work in order to provide an exhaustive methodology for an all-embracing visual rope inspection.

References

1. Zhang, D.L., Cao, Y.N., Wang, C., Xu, D.G.: A New Method of Defects Identification for Wire Rope Based on Three-Dimensional Magnetic Flux Leakage. Journal of Physics: Conference Series **48** (2006) 334–338
2. Platzer, E.-S., Süße, H., Nägele, J., Wehking, K.-H., Denzler, J.: On the Suitability of Different Features for Anomaly Detection in Wire Ropes. In: Computer Vision, Imaging and Computer Graphics: Theory and Applications (Springer CCIS), Springer (2010) 296–308
3. Platzer, E.-S., Nägele, J., Wehking, K.-H., Denzler, J.: HMM-Based Defect Localization in Wire Ropes - A New Approach to Unusual Subsequence Recognition. In: Proceedings of the 31st Annual Symposium of the German Association for Pattern Recognition (DAGM). (2009) 442–451
4. Eisert, P.: Model-based Camera Calibration Using Analysis by Synthesis Techniques. In: Proceedings of the Vision, Modeling, and Visualization Conference (VMV), Aka GmbH (2002) 307–314
5. Koeser, K., Bartczak, B., Koch, R.: An Analysis-by-Synthesis Camera Tracking Approach Based on Free-Form Surfaces. In: Proceedings of the 29th Annual Symposium of the German Association for Pattern Recognition (DAGM), Springer (2007) 122–131
6. Wuest, H., Wientapper, F., Stricker, D.: Adaptable Model-Based Tracking Using Analysis-by-Synthesis Techniques. In: Proceedings of Computer Analysis of Images and Patterns (CAIP), Springer (2007) 20–27
7. Moeslund, T.B., Hilton, A., Krüger, V.: A Survey of Advances in Vision-based Human Motion Capture and Analysis. Computer Vision and Image Understanding **104** (2006) 90–126
8. Hasler, N., Rosenhahn, B., Asbach, M., Ohm, J.-R., Seidel, H.-P.: An Analysis-by-Synthesis Approach to Tracking of Textiles. In: Proceedings of the IEEE Workshop on Motion and Video Computing, IEEE Computer Society (2007) 25

9. Penney, G.P., Weese, J., Little, J.A., Desmedt, P., Hill, D., Hawkes, D.J.: A comparison of similarity measures for use in 2-D-3-D medical image registration. IEEE Transactions on Medical Imaging **17** (1998) 586–595
10. Feyrer, K.: Wire Ropes: Tension, Endurance, Reliability. Springer, Berlin (2007)
11. Shitkow, D.G., Pospechow, I.T.: Drahtseile. VEB Verlag Technik Berlin (1957)
12. Moll, D.: Innovative procedure for visual rope inspection. Lift Report **29** (2003) 10–14
13. Gupta, R., Hartley, R.: Linear Pushbroom Cameras. IEEE Transactions on Pattern Analysis and Machine Intelligence **19** (1997) 963–975
14. Press, W., Teukolsky, S., Vetterling, W., Flannery, B.: Numerical Recipes in C. 2nd edn. Cambridge University Press, Cambridge, UK (1992)
15. McGill, R., Tukey, J., Larsen, W.A.: Variations of Boxplots. The American Statistician **32** (1978) 12–16